SCIENCE SET
OPEN ACCESS PUBLISHERS

Research Article

Journal of Autonomous Vehicles, Drones, and Intelligent Mobility

Hybrid Multi Objectives Optimization Based (TIB -LIB) Constraints to Optimizing GTAW Parameters for Enhancing Microstructure

Abobakr Alsufyani

Industrial and manufacturing system engineering ,king saud university KSA, Saudi Arabia

***Corresponding author:** Abobakr Alsufyani, Industrial and manufacturing system engineering ,king saud university KSA, Saudi Arabia.

Submitted: 19 November 2025 **Accepted:** 25 November 2025 **Published:** 29 November 2025

https://doi.org/10.63620/MKJAVDIM.2025.1006

Citation: *lsufyani, A. (2025). Hybrid Multi Objectives Optimization Based (TIB -LIB) Constraints to Optimizing GTAW Parameters for Enhancing Microstructure. J of Aut Veh Dro and Int Mob, 1(2), 01-12.*

Abstract

This study presents an integrated optimization framework for Tungsten Inert Gas (TIG) welding of AISI 316L stainless steel, combining factorial design, (ANOVA), 2FI model, and DFA to achieve simultaneous optimization of hardness and impact toughness. The hybrid multi-objective approach establishes predictive models validated through experimental confirmation tests to ensure accuracy and consistency of results. Full factorial design experiments were conducted to evaluate the influence of welding current, voltage, and gas flow rate on weld quality. ANOVA results indicated that welding current and voltage were the most significant factors affecting mechanical properties. Using the desirability function, the multi-response objectives were consolidated into a single optimization metric, achieving a composite desirability of welding joint performance of 0.90. Optimal parameters of 165.9 A current, 12.16 V voltage, and 30 CFH gas flow rate produced a weld hardness of 36.4 HRC and an impact toughness of 73.5 J, demonstrating excellent agreement between predicted and experimental results, with SE below 0.04%.the results highlights the effectiveness of integrating RSM and desirability analysis for process optimization, enabling accurate prediction of mechanical responses while reducing experimental complexity. The proposed methodology provides a robust foundation for automated, data-driven control of welding parameters, promoting enhanced weld integrity and sustainable industrial manufacturing practices.

Keywords: TIG Welding, Optimization, Two Factors Interaction Model (2FI) Desirability Function Analysis (DFA), RSM , ANOVA, AISI 316L Stainless Steel, Hardness, Toughness, V-Charpy impact, Fractography, SEM.

Abbreviations

The following abbreviations are used in this manuscript:

TIG: Tungsten Inert Gas
2FI: Two Factors Interaction Model
GTAW: Gas Tungsten Arc Welding
HAZ: Heat Affected Zone
SE: Standard Error
CDF: Composite desirability function
RSM: Response Surface Methodology
DOE: Design of Experiments
DFA: Desirability Function Analysis
SIB: Small is better
LIB: Large is better
TIB: Target Is Better
ANN: Artificial Neural Network
GA: Genetic Algorithm
CFH: Cubic Feet per Hour
BM: Base Metal
WM: Weld Metal
CGHAZ: Coarse-Grained Heat Affected Zone
FGHAZ: Fine-Grained Heat Affected Zone
ICHAZ: Intercritical Heat Affected Zone
SCHAZ: Subcritical Heat Affected Zone
CVN: Charpy V-Notch
DCEN: Direct Current Electrode Negative
SEM: Scanning Electron Microscope
ANOVA: Analysis of Variance

Introduction

Optimization of welding process parameters to achieve the desired weld quality and enhance mechanical properties is essential, as these parameters play a critical role in determining the overall weld quality and service life (durability) of the joint. Since the welding process often involves multiple, sometimes conflicting, objectives, the task of identifying the best combination of parameters constitutes a multi-objective optimization problem. Therefore, it is crucial to determine the appropriate weld input parameters for each new welded product to ensure that the resulting joint meets the required performance specifications and quality standards, [1]. The weld quality reflects the ability of a welded joint to meet the functional requirements of the structure throughout its service life. This includes performance under static or dynamic loading, corrosion resistance, and surface appearance [2]. The quality of a weld is primarily governed by the surface integrity of the weld metal and the heat-affected zone (HAZ), both of which are directly influenced by the type of welding process and its operating parameters. Consequently, welding parameters play a crucial role in determining weld quality, which can be assessed through characteristics such as weld-bead geometry, mechanical properties, and the microstructural condition of the HAZ [2]. Various optimization methods can be applied to define the desired output variables through developing mathematical models to specify the relationship between the input parameters and output variables of the welding process [3]. The application of Design of Experiments (DoE), evolutionary algorithms, and computational intelligence techniques is widely employed to establish mathematical relationships between welding process input parameters and the resulting output responses of the weld joint. These approaches enable the identification of optimal welding conditions that achieve the desired weld quality. Ultimately, the appropriate welding parameters can be selected to produce a joint that most accurately satisfies the required performance specifications. In other words, for every welding process, there exists an ideal combination of parameters that can yield superior weld quality—provided it can be accurately determined through systematic optimization [4]. Accordingly, welding is typically performed with the goal of producing joints that exhibit excellent mechanical properties. To identify the optimal combination of welding parameters that achieve these desired properties, various analytical and computational approaches have been employed. These include Factorial Design, Response Surface Methodology (RSM), Artificial Neural Networks (ANNs), metaheuristic optimization techniques, and hybrid combinations of these methods. Such approaches are widely used to optimize the welding process and ensure that the resulting joints meet the targeted mechanical performance and quality standards.

Materials and Methods

The process parameters were chosen as which are expected to have a significant influence on the measurable outputs. To decide on parameters' levels, screening experiments were conducted and measure, the level values was tuning using DFA, the experimental parameters presented in Table 1 were selected after tuning the parameters to avoid results performance failure.

Table 1: Welding parameters and their levels

				Levels		
Parameters	Code	Notation	Unit	1	2	3
Welding current	A	C	Amber	130	155	180
Welding voltage	B	V	Volt	12	14	16
Gas flow (CFH)	C	GF	CFH	20	25	30

Experiment Materials

The base material used in the present study consisted of AISI 316L stainless steel plates with dimensions of 100 mm × 50 mm × 5 mm, cut from a cold-rolled sheet. The filler material was an ER308 stainless steel solid electrode with a diameter of 2.4 mm. The chemical compositions of both the base metal and the filler are presented in Table 2.

Table 2: Chemical composition of stainless steel AISI316 L & filler metal ER308L

	Chemical composition of stainless steel AISI316 L									
Baseplate	**C**	**Mn**	**Si**	**p**	**Cr**	**Ni**	**Mo**	**Cu**	**Al**	**S**
316 L	0.03	1.74	0.58	0.012	18.5	12	0.2	0.19	0.01	0.01
Filler metal	Chemical composition of filler metal ER308									
ER308	0.05	1.68	0.53	0.018	19.45	9.0	0.116	0.082	0.01	0.03

The impact test was performed at room temperature using a pendulum-type impact testing machine with a maximum capacity of 250 J, as shown in Figure 6. ASTM E23-04 specifications were followed for both specimen preparation and testing. A V-groove joint design was employed, and welding was completed in a single pass to ensure full penetration. Prior to welding, all edges were thoroughly cleaned mechanically and chemically to eliminate any potential sources of contamination, including rust, scale, dust, oil, and moisture.

Table 3: welding condition

Polarity	DCEN
Filler Materials	ER308
Electrode Diameter	2.4mm
Shielding Gas Torch	99% Argon

Position Operation	horizontal (F1) .
Operation	TIG-Semi automatic(manual)
Joint type	Butt-V groove

The key factors that significantly influence the mechanical properties and weld quality characteristics in Gas Tungsten Arc Welding (GTAW) have been identified and considered in this study. These factors include welding voltage, current, and shielding gas flow rate. After tacking the plates, the weld pass was carried out using the GTAW process under the welding conditions listed in Table 3. The overall methodology was implemented following the sequence illustrated in Figure 1.

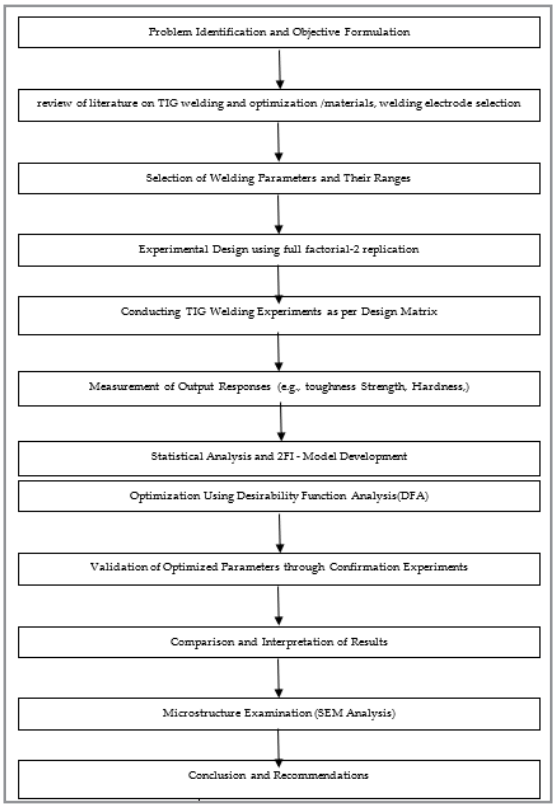

Figure 1: Methodology of Experiment

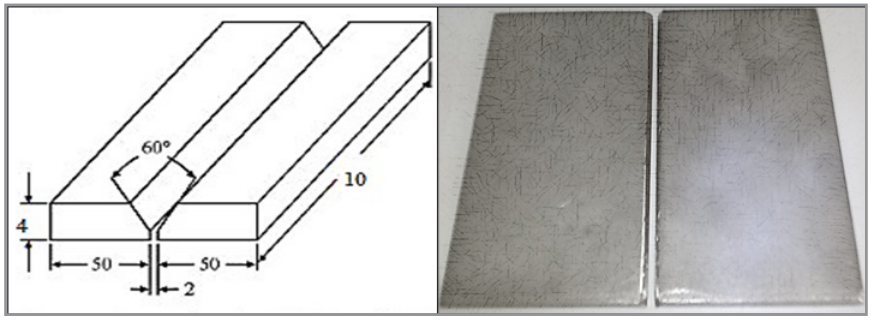

Figure 2: Welding Configuration joint (Dimensions in cm).

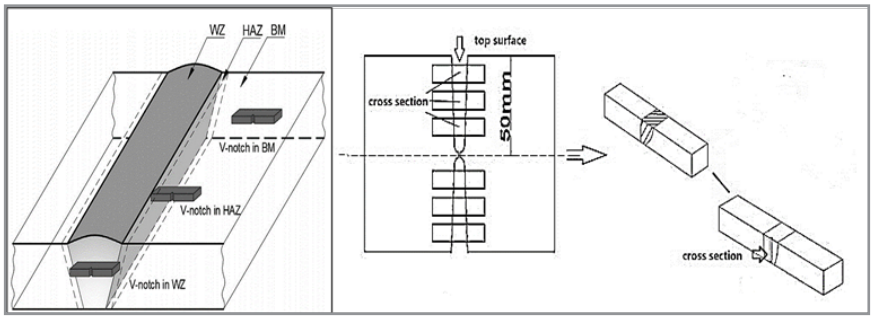

Figure 3: The welded joints sampling for impact test specimens.

The confirmation tests of the welded specimens were conducted and analyzed at ambient temperature across the distinct metallurgical zones, namely the Weld Zone (WZ), Heat-Affected Zone (HAZ), and Base Metal (BM), to evaluate the impact properties. No preheating or post-weld heat treatment was applied prior to testing. The Gas Tungsten Arc Welding (GTAW) process was performed manually under controlled conditions, with continuous visual inspection throughout the welding operation to ensure weld integrity and uniform bead geometry. All welds demonstrated satisfactory surface appearance, with no detectable defects such as porosity, blowholes, or undercuts. The hardness distribution across the welded joint was measured using the Rockwell hardness test (Scale C) with a 1 mm diamond indenter, following a defined contour line across the WZ, HAZ, and BM regions.

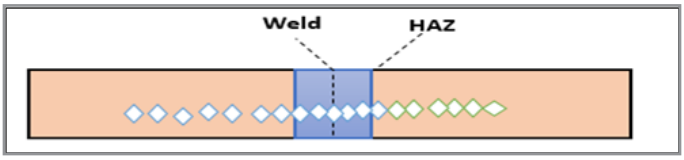

Figure 4: Schematic Diagram of hardness Test

Discussion & Results

Tungsten Inert Gas (TIG) welding was performed in the welding workshop using a standard TIG welding machine. A total of 27 experimental runs were carried out, each replicated twice, resulting in 54 welded specimens. All welds were executed by qualified and certified welders to ensure sound weld quality and process reliability. Hardness testing was conducted on the various welded specimens, with five sets of readings obtained for each condition, and the average values were used for analysis. The Rockwell hardness measurements were performed using a Zwick-type Rockwell Hardness Tester at ambient temperature, applying a major load of 150 kgf. The hardness values were recorded on the Rockwell C scale (HRC) and used to evaluate and optimize the welding parameters. The hardness of the base metal was also measured to serve as a reference for comparative analysis, as presented in Table 4.

Table 4: Base metal hardness-HRC

S. N	Sample - no	Rep 1	Rep 2	Rep 3	Rep 4	Rep 5	Average	St deviation
1	Sample -1 (HRC)	36	36.3	36.2	35.9	36.2	36.12	0.16431677
2	Sample -2 (HRC)	37	36.4	36.6	36.5	36.5	36.6	0.23452079
	Total average						36.36	

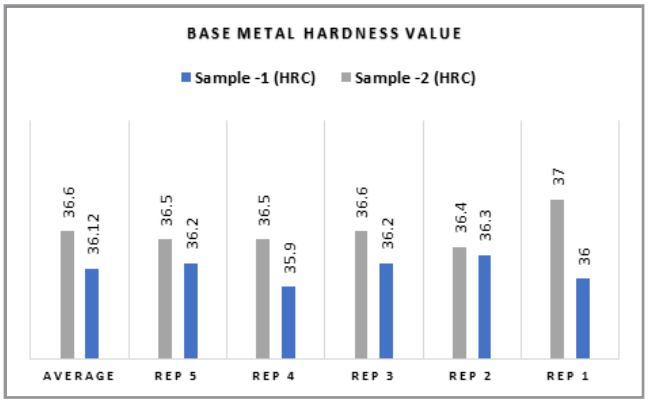

Figure 5: Base metal hardness results

V- Charpy Impact of Base Metal

Higher absorbed energy indicates a tougher material, which is less likely to fail catastrophically under mechanical shocks or impacts. The Charpy impact energy values of the base metal are presented in Table 5.Table 5 V- Charpy impact toughness results of base metal.

Figure 6: specimens conducted - V impact test

Sample No	impact value (joules)
Specimen 1	65
Specimen 2	69
Specimen 3	66.4
Specimen 4	61.2
Specimen 5	63.8

The V-notch Charpy impact energy of the unwelded base metal ranged between 61 J and 69 J, as presented in Table 5, with an average value of 65 J and a standard deviation of 3.3 J. The preparation of the specimens, both before and after testing, is shown in Figure 6.

2FI - Model with Desirability Function Analysis

In this study, Tungsten Inert Gas (TIG) welding parameters were optimized using a Two-Factor Interaction (2FI) model integrated with Desirability Function Analysis (DFA). The aim was to achieve a balanced performance where hardness follows a "target-is-best" criterion, ensuring sufficient joint strength, while impact toughness follows a "larger-is-better" objective to enhance ductility and energy absorption, particularly in cryogenic or low-temperature applications. The input parameters considered for the optimization included welding current (A), arc voltage (V), and welding speed (mm/s). These process parameters were selected based on their significant influence on heat input, grain refinement, and metallurgical transformations in the fusion and heat-affected zones[5][6]. The experimental design followed a Response Surface Methodology (RSM) with a 2FI regression model to evaluate the interactive effects between parameters on the responses. The mathematical 2FI model established was expressed as:

$Y = \beta_0 + \Sigma\beta_i X_i + \Sigma\beta_{ij} X_i X_j + \varepsilon$

where Y represents the response (hardness or impact energy), X_i are the coded input variables, and β coefficients represent linear and interaction effects. Desirability Function Analysis was applied to integrate both objectives into a single composite desirability index (D). The individual desirability (d_1 for hardness and d_2 for impact energy) were computed as follows:

- For hardness (target is best): $d_1 = 1 - |(Y - T)| / \Delta T$, where T is the target hardness value.
- For impact energy (larger is better): $d_2 = (Y / Y_{max})$.

The overall desirability was then calculated as D = (d_1 × d_2)^(1/2), allowing simultaneous optimization of both mechanical properties. The optimized TIG parameters corresponded to high current and moderate welding speed, providing optimal fusion without excessive grain coarsening.

The developed 2FI-DFA approach demonstrated effective multi-response optimization, ensuring a robust welding process with an ideal trade-off between hardness and impact toughness. This method provides a systematic framework for parameter tuning in TIG welding of stainless steels and other structural alloys used in cryogenic and high-integrity applications. The statistical software Minitab 17.0 is employed to investigate the significance and interaction of welding parameters, namely welding current, voltage and gas flow rate. ANOVA is calculated for analyzing the importance of process parameters. The least-squares method is used to construct a regression equation relating each process output with the variable process parameters. The 2FL model is usually of the form:

$$Y = \beta_o + \sum_{i=1}^{k} \beta_i X_i + \sum\sum_{i<j} \beta_{ij} X_i X_j \qquad \text{Eq.1.1}$$

Where Y is the response under consideration, β_0 is the constant term, β_i represents the linear effects, and β_{ij} represents the second-order interaction effects. The ANOVA results indicate that all input parameters have a significant effect on the impact strength of the welded joint, and significant interactions between parameters were also observed for impact toughness at a confidence level of 0.05. The residuals represent the fitting error, i.e., the difference between the actual sample values and the predicted estimates. The Normal Probability Plot of the residuals for hardness is shown in Figure 7, which demonstrates that the residuals lie approximately along a straight line, indicating that the errors are normally distributed. Additionally, the assumption of constant variance was verified using the residuals versus fitted values plot.

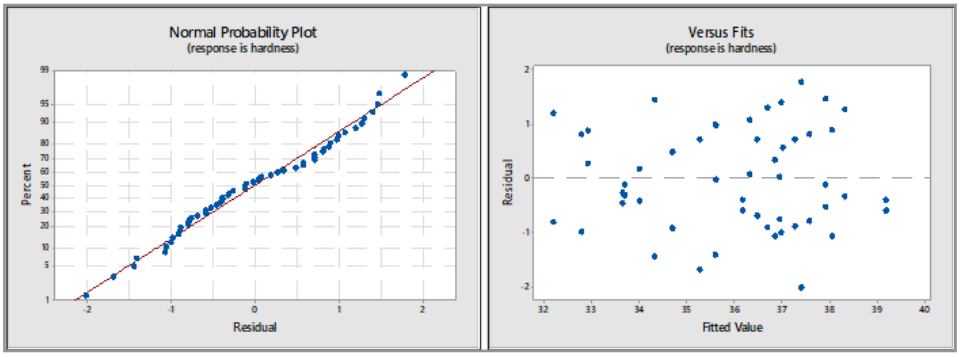

Figure 7: The residuals plot of hardness values

The above plot shows a random pattern of residuals on two sides of the zero line, and it should

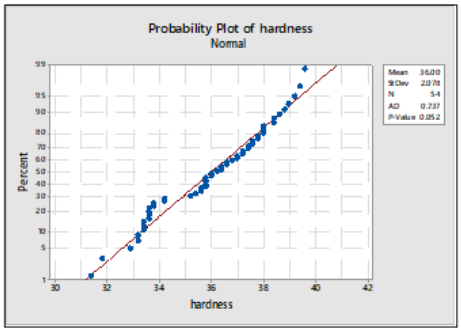

Figure 8: Normality Plot of the Hardness

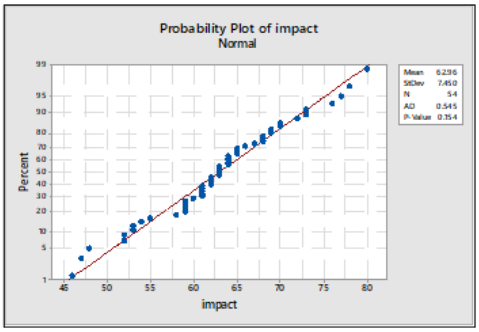

Figure 9: Probability plot of toughness

The residuals do not exhibit any recognizable patterns or unusual structures, indicating randomness. A general observation is that residuals tend to increase slightly as the fitted values increase, which is common in experimental data. The Anderson–Darling test yielded a p-value of 0.052 (> 0.05), confirming that the residuals are normally distributed, as shown in Figure 8.Hardness testing was performed on various welded specimens, and ANOVA results identified that the most influential factor affecting hardness is the welding current, with its first level at 130 A. The second most significant factor is the gas flow rate, at its third level of 30 CFH. The second-order interaction (2FI) model for hardness is expressed as:

hardness (A,B,C) = -32.3 + 0.1449 current(A) + 3.090 voltage(B) + 2.750 gas(C) - 0.00697 current(A)*gas(C) - 0.1121 voltage(B)*gas(C).

The ANOVA results indicate that all input parameters have a significant effect on the impact strength of the welded joint, and significant interactions between parameters were also observed for impact toughness at a significance level of 0.05. The coefficient of determination (R^2) was used to assess the goodness of fit of the model, indicating how closely the predicted values align with the experimental data. The corresponding R^2 values for the impact tests are provided in the results.

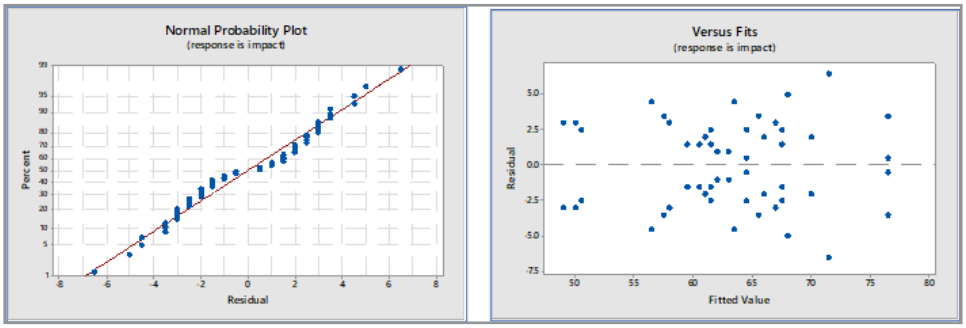

Figure 10: The residuals plot of toughness

The model yielded an R^2 value of 84.16% and an adjusted R^2 of 78.91%, indicating that the designed model has a good fit and is valid for further investigation. The probability plot confirms the normality of the data, as most points closely follow the straight line with minimal residual deviation. Figure 10 presents the residuals versus fitted values and observation order, showing that the residuals are randomly distributed with no discernible pattern.

The Anderson–Darling test resulted in a p-value of 0.154 (> 0.05), further confirming that the residuals are normally distributed, as shown in Figure 23. Impact testing was conducted on various welded specimens, and the corresponding mathematical model for toughness is expressed as:
Absorbed energy (A,B,C) = -285.7 + 0.929 current(A) + 23.73 voltage(B) + 8.37 gas(C) - 0.0625 current(A)*voltage(B) - 0.575 voltage(B)*gas(C).

DFA & RSM Optimization.
Design Expert 12.0 was used to develop the experimental plan for Response Surface Methodology (RSM). RSM was applied to optimize welding parameters with the objective of maximizing both hardness and impact strength, as illustrated in Figure 11.

The analysis indicates that lower welding current and voltage maximize hardness because high heat input adversely affects the microstructure, leading to coarse grains, which reduce hardness. Additionally, hardness increases with higher gas flow rates, as shielding gases prevent atmospheric contamination, reduce oxidation, and improve the mechanical properties of the weld joint.

The 3D surface plots illustrate these relationships. In the plot of current and gas flow rate versus hardness, when current varies from 130 A to 165.5 A, hardness reaches its optimal value as gas flow rate increases from 20 to 30 CFH. Figure 11(a) shows the interaction between current, voltage, and gas flow rate with the response variable (hardness). For example, an optimal hardness of 36.3 HRC was recorded at 12.1 V and 30 CFH. Figure 11(b) presents the interaction effect of gas flow rate versus current on hardness, showing that low current combined with high gas flow maximizes hardness.

The response surface plots further demonstrate how hardness varies with changes in each welding parameter relative to their reference points. Similarly, low welding current and voltage maximize impact toughness, since excessive heat input leads

to coarse grains that reduce toughness. Impact strength also increases with higher gas flow rates. The interaction effect of gas flow versus current on impact toughness is presented in Figure 12, illustrating the combined influence of these parameters on weld performance. It can be seen that increasing gas flow increases impact from 48 to 73.3 as optimum value, and it Higher current and voltage levels negatively affect impact toughness, as they increase heat input, leading to microstructure coarsening and a slight reduction in the mechanical properties of the weld. As the heat input rises (with higher voltage and current), the impact toughness of the welded joint decreases slightly due to grain growth in the microstructure.

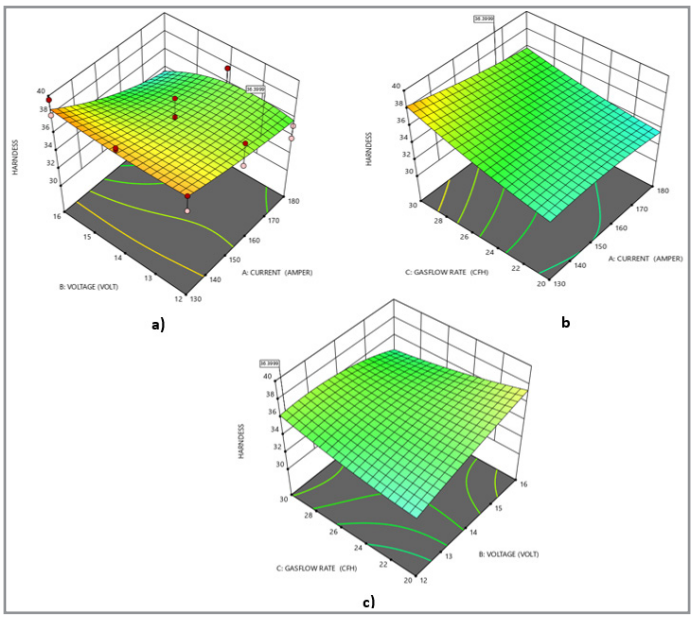

Figure 11: shows the interaction plot of process parameters and their effects on the hardness

Figure 11(c) shows the surface plot of voltage and gas flow rate versus impact toughness. When voltage varies from 12 V to 12.16 V, the impact toughness reaches its maximum value. Additionally, increasing the gas flow rate from 20 to 30 CFH further enhances the impact value. Shielding gases with low ionization potential promote stable arc ignition, while gases with low thermal conductivity help maintain arc stability, contributing to improved mechanical performance.

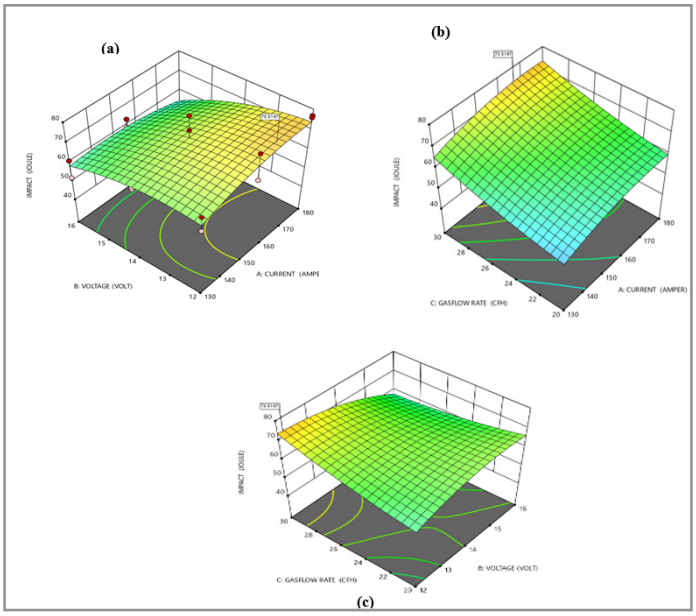

Figure 12 (a), (b) , (c): Response surface graphs of process parameters on the absorbed energy

When there are multiple response variables, it is necessary to determine a set of factor settings that simultaneously optimizes all responses according to specified criteria, since a factor setting that is optimal for one response may not be optimal for another. The desirability function is used to identify the best overall factor settings, with the overall desirability (D) quantifying how well the combined goals for all responses are satisfied. The 'optimal' factor settings are those that maximize the overall desirability. In this study, Design Expert 12.0 software was employed to perform the optimization, with constraints for the optimization provided in Table 8. The optimized results, along with their corresponding desirability values, are reported, and the set of process parameters yielding the maximum overall desirability was selected for implementation.

Within 28 iterations, and according to the specified constraints, the optimization targeted a hardness value of 36.4 HRC (matching the base metal to ensure surface integrity) and an impact

strength of 73.5 J as the optimal values. Graphical optimization enables visual selection of the optimum welding parameters within the defined constraints (Figure 13).

In this study, there are two competing response variables—hardness and impact strength—used to determine the optimal welding parameters. The predicted maximum values of the responses were impact energy = 75.3 J and hardness = 36.4 HRC, with individual desirabilities of 0.81 and 1.0, respectively, resulting in a composite desirability of 0.90 (90%), as shown in Figure 31. The use of RSM facilitates the optimization of welding process variables to achieve the most favorable mechanical properties and microstructural integrity of the weld joint.

Table 6: Optimization constraints table

Name	Constraints	Lower Limit	Upper Limit	Lower Weight	Upper Weight	Importance
A: current	is in range	130	180	1	1	3
B: voltage	is in range	12	16	1	1	3
C: gas flow rate	is in range	20	30	1	1	3
Hardness	is target = 36.4 (TIB)	31.4	39.6	1	1	3
Impact	Maximize(LIB)	46	80	1	1	3

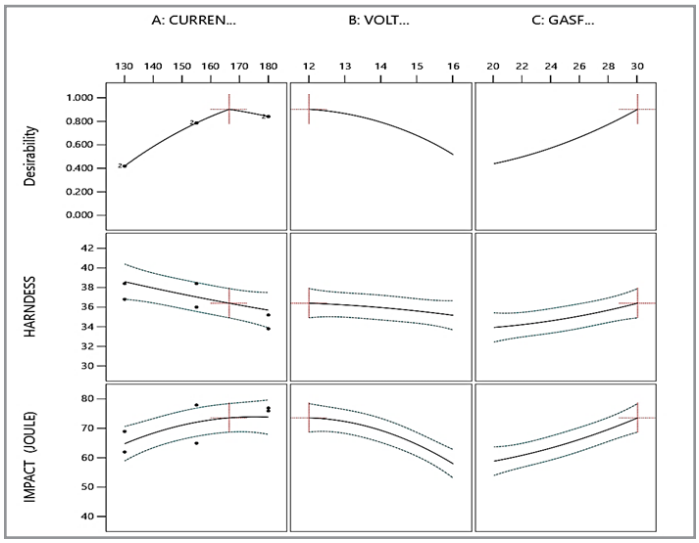

Figure 13: Graphical plot of DFA

Based on the optimal solution, the response surfaces illustrate the relationship between desirability values and the optimized input variables. The optimization problem was solved using composite desirability, resulting in a composite desirability value of D = 0.90, which identifies the factor settings that simultaneously optimize all response variables.

Table 7: The hardness results of the confirmatory test

Item	Welding Zone (Hardness – HRC)	Average	Predicted	Percent Error
Specimen 1	39.2, 39.5, 37.6, 38.2, 35.1, 37.92	36.4	36.4	0.04
Specimen 2	38.7, 36.6, 37.9, 35.6, 39.4, 37.64	36.4	36.4	0.03

The optimal factors setting are 165.9 of welding current, 12.16 volts of voltage and 30 CFH of gas flow.

The quality of a welded joint is directly influenced by the welding input parameters. Inadequate variable welding parameters such as Welding Current, welding voltage and gas flow rate may contribute to the failure of a welded structure which determines stress and impact toughness capacity of a welded joint. The optimum range of input variables that produced the desired process output was estimated through the use of composite desirability function. Using desirability function, we can obtain an optimal setting which maximizes all response variables of hardness and impact test. After the optimal parameters have been selected, the final step is to predict and verify the improvement of the quality characteristic using the optimal level of design parameters. The optimized parameters have been verified by conducting and producing three confirmatory samples and to be tested at room and cryogenic temperatures. After the welding, the samples were sectioned, then testing measured and record in three-zone (parent metal, heat affected zone and welding zone), on the room temperature for impact test, and hardness test.

Validation Through Confirmation Experiments

The hardness results from the confirmatory tests are presented in Figure 14, demonstrating that the predicted optimal parameter settings are valid. The confirmatory tests were conducted using the optimal combination of welding parameters to verify the predicted mechanical characteristics. The results show that the optimum welding conditions produced hardness values that closely matched the predicted values, with a percent error of only 0.03%, confirming the accuracy and reliability of the proposed optimization methodology.

The numerical optimization of current, voltage, and gas flow rate proved effective, as the predicted hardness responses were very close to the actual values required to achieve optimum welds with minimal defects. Similarly, confirmatory tests were conducted to validate the impact response under the predicted optimal parameters. The results indicate that the desirability-based optimization technique effectively optimizes TIG welding of stainless steel, as the actual and predicted impact values were in close agreement, with a percent error of 0.034%, as summarized in Table 8.

Table 8: v- Charpy Impact test confirmation

Item (room temperature)	Specimen 1	Specimen 2	Average value	Predicted value	Percent error
Welding zone –impact value	79.5	66.6	73.05	73.3	0.003411

It was observed that a welding current of 165.9 A, voltage of 12.16 V, and gas flow rate of 30 CFH produced a weld joint with high impact strength. This combination was identified by Design Expert as the optimal solution for achieving the desired mechanical properties.

Discussion of Confirmation Experiments

The hardness measurements were taken on the Rockwell HRC scale with a 150 kgf load and are plotted in Figure 14, showing the hardness distribution across the welded joints of the AISI 316L steel plates. Hardness is a key parameter for evaluating cold cracking resistance, strength, ductility, and toughness, so measurements were taken along a straight line across the top surface, covering the Weld Metal (WM), Heat-Affected Zone (HAZ), and a portion of the Base Metal (BM).The hardness profile showed minimal variation. The peak hardness in the fusion zone was 49 HRC for specimen No. 1 and 47.9 HRC for specimen No. 2, with all measured values above 38 HRC. The HAZ and weld regions exhibited slightly higher hardness for both specimens, which remains acceptable. The weld zone, from –3 mm to +3 mm, displayed a relatively homogeneous hardness, with a slight increase at the boundary between the WM and HAZ.

This pattern is consistent with typical welding behavior, where hardness is higher near the top of the weld bead surface and gradually decreases toward the center of the fusion zone. This occurs because the cooling rate is higher at the top surface of the weld bead than at the center of the weld metal, leading to localized hardening at the surface.

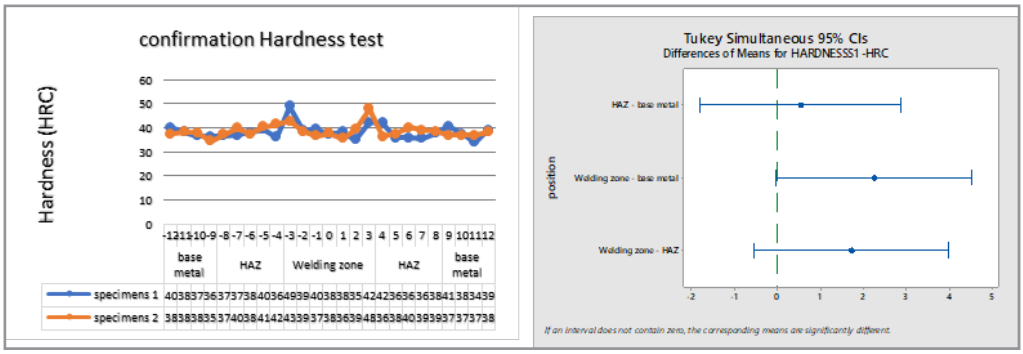

Figure 14: surface integrity confirmation.

Figure 15: Tukey test of hardness on (WZ, HAZ, BM).

The high hardness observed at the fusion boundary zone (FBZ) in all joints can be attributed to the presence of partially unmelted grains at the fusion boundary, which act as nucleation sites for the newly precipitating phase of the weld metal during solidification. After reaching this peak hardness, the microhardness gradually decreases in the Heat-Affected Zone (HAZ).

Within the HAZ, the region adjacent to the fusion boundary is the Coarse-Grained HAZ (CGHAZ), which exhibits lower hardness, while the region adjacent to the base metal is the Fine-Grained HAZ (FGHAZ), exhibiting higher hardness. This trend is due to differences in cooling rates: the CGHAZ near the fusion zone cools relatively slowly, resulting in coarse grains, whereas the FGHAZ near the base metal experiences faster cooling due to steeper thermal gradients, producing fine grains [7].

As shown in Figure 14, the hardness across the Weld Zone (WZ), HAZ, and Base Metal (BM) demonstrates uniform surface integrity, with no significant differences between regions (p-value = 0.052 > 0.05).

V-Notch Charpy impact tests were performed in the three zones of the welded joint: Weld Metal (WM), HAZ, and Parent Metal (PM). For each zone, three specimens were tested according to ASME IX and ASME II-Part A SA370 standards at ambient temperature. The impact tests provide additional insights into the toughness characteristics of the weldments. Triplicate testing was conducted to account for the inherent variability in weld properties.

Table 11 presents the Charpy-V impact test results for two samples, each tested at three locations within the weld zone, HAZ, and base metal. The tests were conducted along the weld centerline and demonstrate that all weldments satisfy the BV and DNV acceptance criteria, confirming adequate toughness and mechanical performance across all critical zones [8].

Table 9: V- Charpy Impact results of the confirmation test

V- Impact results of the confirmation test– (J).			
	Base Metal	**HAZ**	**Welding zone**
Specimens 1	69.0	98.3	79.5
Specimens 2	65.0	103.2	92.2
Average	67	100.75	85.85

The Heat-Affected Zone (HAZ) exhibited the highest impact toughness in both specimens, with values ranging from 98.3 J to 103.2 J, representing an increase of approximately 43–59% compared to the base metal. This enhancement suggests that grain refinement or partial annealing occurred due to the thermal cycle of welding. Figures 21 and 22 provide a clear comparison of the confirmatory results. The Weld Zone (WZ) demonstrated moderate toughness, with values between 79.5 J and 92.2 J, which is 15–42% higher than the base metal. Despite the effects of solidification, the WZ maintains reasonable ductility, confirming good mechanical performance of the welded joint

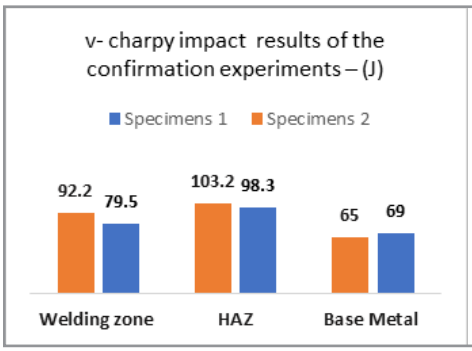

Figure 16: V-charpy Impact test

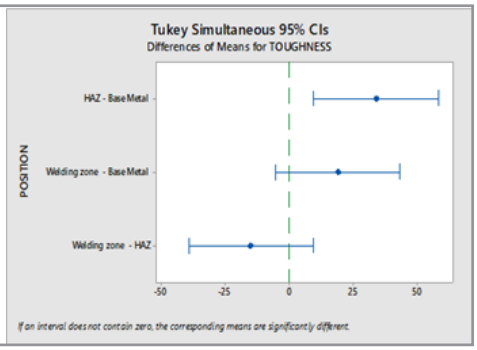

Figure 17: Tukey test Of Absorbed Energy

The Base Metal shows lowest impact toughness (65–69 J), serving as the reference baseline (100%). It indicates higher brittleness and less ability to absorb impact energy.

Welding Zone

Impact toughness: 92.2 J (Specimen 1) and 79.5 J (Specimen 2). The welding zone shows moderate toughness, but slightly lower than the HAZ region. Indicates some loss of ductility due to weld metal solidification and microstructural changes.

Heat-Affected Zone (HAZ)

Highest impact toughness among the three regions: 103.2 J (Specimen 1) and 98.3 J (Specimen 2). This means the HAZ region absorbed more energy before fracture, showing better toughness due to refined grain structure or partial annealing effects during welding.

Base Metal

Lowest impact toughness: 65 J and 69 J. Suggests the parent metal is more brittle compared to welded or heat-affected areas. This might occur if the base metal has not undergone thermal refinement or contains inherent impurities or coarser grains. on Figure 16, Figure 17 , could be understood that the absorbed energy of V- charpy test on the different positions of HAZ,W-Z,BM no strong significance differences between them with p Value 0.76 > 0.05 , therefore ,it has concluded main effects of optimizing TIG welding parameters on enhancing the toughness and mechanical properties totally.

- HAZ region → Exhibits the best toughness and energy absorption capacity.
- Welding zone → Moderate performance, slightly below HAZ.
- Base metal → Shows the lowest toughness, likely the most brittle part.

Fractography Discussion

Ductile metals typically exhibit significant plastic deformation and high energy absorption before fracture. In contrast, brittle materials display little to no plastic deformation and low energy absorption during fracture. Any fracture process involves two steps: crack initiation and crack propagation under applied stress. The mode of fracture is strongly influenced by the mechanism of crack propagation.

Ductile fracture is generally preferred over brittle fracture for two main reasons. First, brittle fracture occurs suddenly and catastrophically, without warning, due to rapid crack propagation. In ductile materials, plastic deformation provides early warning that failure is imminent, allowing preventive measures to be taken. Second, ductile fracture requires more strain energy, as these materials are generally tougher [9].

The fracture morphology of the parent metal after V-Notch Charpy impact testing is shown in Figures 18a and 18b. Both images display typical ductile fracture characteristics, with clear evidence of micro-void formation and coalescence, though some localized imperfections are present. In Figure 18a, the fracture surface shows secondary cracks, porosity, and pockets along the fracture path, suggesting localized stress concentrators caused by inclusions or micro-voids formed during material processing [10,11]. The presence of micro-cracks indicates partial brittleness in certain zones, while the overall texture, characterized by shallow dimples, confirms that the parent metal underwent limited plastic deformation prior to failure.

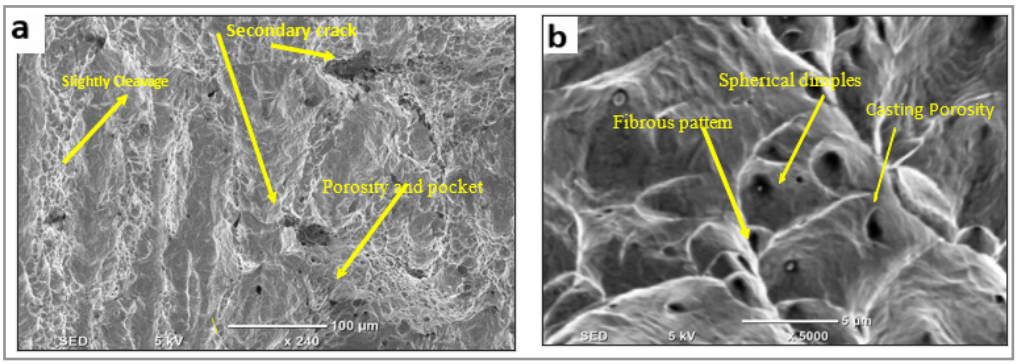

Figure 18: Fracture surface of the impact test - parent metal

Figure 18b shows a more refined fibrous and dimpled fracture surface, featuring spherical dimples, fibrous patterns, and initial porosity. The presence of dimples indicates micro-void coalescence, confirming a predominantly ductile fracture mechanism. However, the small pores and voids may slightly reduce the toughness of the base material.

Overall, both Figures 18a and 18b demonstrate that the parent metal fractured primarily through a ductile mechanism, involving micro-void nucleation, growth, and coalescence. The observed porosity and secondary cracking correlate with the measured impact toughness values of 65–69 J for the base metal, indicating moderate toughness and partial brittleness due to inherent microstructural features [11-13].

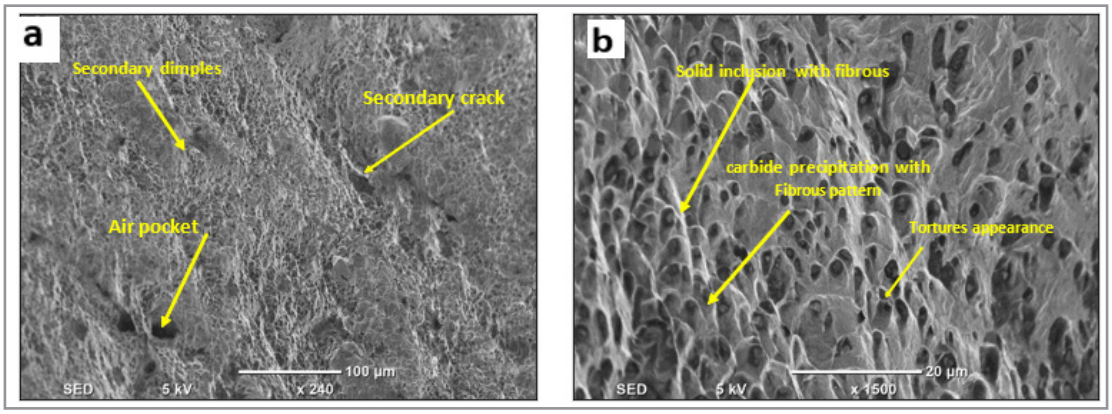

Figure 19: Fracture of the Impact Test– welding joint

The fracture morphology of the welded joint after Charpy impact testing is presented in Figure 19a and Figure 19b. Both micrographs exhibit features characteristic of a ductile fracture mode, including dimples, micro-voids, and secondary cracking, which collectively indicate significant plastic deformation before final failure. In Figure 19a, the surface reveals secondary dimples, air pockets, and secondary cracks distributed irregularly across the fracture zone. These features represent regions of micro-void nucleation and coalescence, which occur due to local plastic strain concentration around inclusions or defects. The presence of secondary cracks and air pockets indicates the initiation of void growth under tensile stress, confirming that the material experienced ductile tearing before separation. Figure 19b displays a more homogeneous fibrous dimple morphology with evident ductile inclusions and tear ridges [7, 14-16]. The rounded and elongated dimples correspond to the direction of crack propagation, confirming extensive plastic deformation. The presence of inclusion particles within dimples further demonstrates that micro-void coalescence was the dominant fracture mechanism. The fibrous appearance indicates energy absorption through plastic deformation, which correlates with the relatively high impact toughness observed experimentally. Overall , both SEM images confirm that the fracture of the welded joint was governed primarily by ductile fracture behavior, involving micro-void nucleation, growth, and coalescence [10, 11, 15, 17]. The absence of cleavage facets or river patterns further supports the lack of brittle fracture. Consequently, the weld exhibits good impact toughness and resistance to sudden fracture, consistent with the absorbed energy values obtained from the Charpy V-notch impact tests.The SEM evidence confirms that optimized TIG welding parameters minimized welding defects such as porosity and micro-cracks while promoting ductile fracture behavior. The resulting fine dimpled surface morphology and absence of brittle cleavage facets indicate a well-balanced heat input, refined grains, and improved metallurgical bonding. Consequently, the optimized weld joint exhibits enhanced mechanical integrity, high impact toughness, and superior performance under dynamic loading. In summary, the SEM analysis in Figures 19a and 19b visually validates that optimization of welding parameters effectively enhances the microstructure and mechanical properties of the welded joint by refining the grain structure, reducing defects, and promoting ductile fracture mechanisms.

Conclusion

The results of this study confirm that the combination of factorial design, ANOVA, and Response Surface Methodology (RSM) integrated with desirability function analysis provides a reliable and efficient optimization framework for TIG welding applications. The optimized parameters 165.9 A current, 12.16 V voltage, and 30 CFH gas flow—produced superior mechanical properties characterized by high hardness (36.4 HRC) and balanced

impact toughness (73.5 J). These findings validate the predictive strength of the developed regression models and demonstrate that the methodology ensures consistent weld quality and mechanical performance with minimal deviation from target responses. Microstructural analysis verified that the optimized parameters resulted in refined and homogeneous grain structures in the fusion and heat-affected zones, improving ductility, surface integrity, and resistance to crack initiation. The confirmation and validation tests showed remarkable consistency, proving the adequacy of the optimization framework and its applicability across varying thermal and service conditions. The study also highlighted the importance of balancing process parameters to maintain microstructural stability and achieve mechanical harmony in welded joints. In conclusion, this research successfully establishes a robust optimization and validation framework that not only enhances the understanding of process-structure-property relationships in TIG welding but also provides a foundation for industrial automation and advanced material design. The integration of experimental validation and numerical prediction offers a pathway toward intelligent, adaptive welding systems and sustainable manufacturing processes. Future work can extend this approach to dissimilar materials, hybrid welding processes, and real-time control systems to further advance process optimization and mechanical reliability.

References

1. Benyounis, K. Y., & Olabi, A.-G. (2008). Optimization of different welding processes using statistical and numerical approaches: A reference guide. Advances in Engineering Software, 39(6), 483–496.
2. Afshari, D., Sedighi, M., Barsoum, Z., & Peng, R. L. (2012). An approach in prediction of failure in resistance spot welded aluminum 6061-T6 under quasi-static tensile test. Proceedings of the Institution of Mechanical Engineers, Part B: Journal of Engineering Manufacture, 226(6), 1026–1032.
3. Kolahan, F., Manoochehri, M., & Hosseini, A. (2011). Application of Taguchi method and ANOVA analysis for simultaneous optimization of machining parameters and tool geometry in turning.
4. Benyounis, K. Y., Olabi, A.-G., & Hashmi, M. S. J. (2008). Multi-response optimization of CO_2 laser welding process of austenitic stainless steel. Optics & Laser Technology, 40(1), 76–87.
5. Limon-Romero, J., Baez-Lopez, Y., Tlapa, D., & Pory-Lugo, M. (2017). Optimization of multiple response variables using the desirability function and a Bayesian predictive distribution. International Journal of Industrial Engineering, 132, 85–95.
6. Ayinavilli, S. (2018). Taguchi based desirability function analysis for the optimization of multiple performance characteristics. International Journal of Modern Trends in Engineering and Research, September. https://doi.org/10.21884/IJMTER.2018.5157.FY4QK
7. Kumar, S., & Shahi, A. S. (2011). Effect of heat input on the microstructure and mechanical properties of gas tungsten arc welded AISI 304 stainless steel joints. Materials & Design, 32(6), 3617–3623.
8. Blodgett, O. W., Funderburk, R. S., Miller, D. K., & Quintana, M. (1999). Fabricators' and erectors' guide to welded steel construction (pp. 42–44). James F. Lincoln Arc Welding Foundation.
9. Callister, W. D., & Rethwisch, D. G. (2009). Materials science and engineering: An introduction (8th ed.). Wiley.
10. Waqas, A., Qin, X., Xiong, J., Zheng, C., & Wang, H. (2019). Analysis of ductile fracture obtained by Charpy impact test of a steel structure created by additive manufacturing.
11. Belyakov, A. (2018). Microstructure and mechanical properties of structural metals and alloys. Metals, 8(9). MDPI.
12. Spanos, G., Fonda, R. W., Vandermeer, R. A., & Matuszeski, A. (1995). Microstructural changes in HSLA-100 steel thermally cycled to simulate the heat-affected zone during welding. Metallurgical and Materials Transactions A, 26(12), 3277–3293.
13. Kalpakjian, S., Schmid, S. R., & Musa, H. (2017). Manufacturing engineering and technology (6th ed.). Prentice Hall.
14. Wang, X.-N., Zhang, S.-H., Zhou, J., Zhang, M., Chen, C.-J., & Misra, R. D. K. (2017). Effect of heat input on microstructure and properties of hybrid fiber laser–arc weld joints of the 800 MPa hot-rolled Nb–Ti–Mo microalloyed steels. Optics and Lasers in Engineering, 91, 86–96.
15. Wang, W., Lu, Y., Ding, X., & Shoji, T. (2015). Microstructures and microhardness at fusion boundary of 316 stainless steel/Inconel 182 dissimilar welding. Materials Characterization, 107, 255–261. https://doi.org/10.1016/j.matchar.2015.07.018
16. Rr, P. M. (2016). Fractographic analysis of welded joint surfaces. International Journal of Fracture Mechanics, 37(12), 34–37.
17. Lakshminarayanan, A. K., Shanmugam, K., & Balasubramanian, V. (2009). Effect of welding processes on tensile, impact, hardness, and microstructure of joints made of AISI 409M FSS base metal and AISI 308L ASS filler metals. Ironmaking & Steelmaking, 36(1), 75–80.